JMPM: Jurnal Material dan Proses Manufaktur
Vol. 8, No. 1, p16-26, Juni 2024
DOI: https//doi.org/10.18196/jmpm.v8i1.21848

Impact of Mass Flow Rate on Thermal Behavior of PCM-Based SWH during Charging Operations

Muhammad Nadjib[a,*], Wahyudi[a], Tito Hadji Agung Santosa[a], Tegar Bagaskara Febriansyah[a]
[a] Mechanical Engineering Department, Engineering Faculty, Universitas Muhammadiyah Yogyakarta, Jl. Brawijaya Tamantirta, Bantul, Yogyakarta 55163, Indonesia, +62 274 387656
e-mail: nadjibar@umy.ac.id*, wahyudi@ft.umy.ac.id, titohas@umy.ac.id, tegar.bagaskara.ft18@mail.umy.ac.id

Keywords:

Charging efficiency; cumulative heat stored; paraffin wax; solar water heater

ABSTRACT

Using phase change materials in solar water heaters presents an intriguing prospect due to their notable energy density and potential for substantial thermal energy storage capacity. In the context of active-type solar water heaters, careful consideration must be given to the water flow rate as a crucial parameter. This paper investigates the thermal dynamics of active-type solar water heaters equipped with phase change materials, examining variations in mass flow rate during the charging process. Indoor experiments utilized horizontal tanks, flat plate collectors, pumps, and solar simulators. Cylindrical capsules filled with paraffin wax were employed and arranged horizontally within the tank, while K-type thermocouples were utilized to monitor water and paraffin wax temperatures. Charging procedures were executed over 160 minutes with mass flow rate adjustments. Data analysis was performed to evaluate the system's thermal performance during charging. Results indicate higher mass flow rates correspond to increased instantaneous, cumulative heat storage and charging efficiency. The mass flow rate notably affects the thermal efficiency of solar water heater systems incorporating phase change materials.

1. INTRODUCTION

Indonesia's primary energy challenge lies in its heavy reliance on fossil fuels. As of 2021, the country's energy mix is dominated by coal (38.5%), oil (32.8%), and gas (17.4%), with renewable sources accounting for only 11.3% [1]. Without effective intervention, Indonesia may encounter energy supply issues. To address this, the Indonesian government has devised a strategy to curb fossil fuel consumption by bolstering renewable energy's role. The aim is to raise the renewable energy share to 23% by 2025 and 31% by 2050 [2]. Solar energy emerges as a key focus within this renewable energy mix. Leveraging Indonesia's substantial solar potential, with an average insolation value of 4.8 kWh/m^2/day [3], the government's initiative to harness solar power is fitting. This abundant solar resource can serve as a significant energy source, capable of generating electricity or heat through conversion technologies.

Solar water heaters (SWH) are designed to utilize solar energy to heat water. They are classified into two main types based on the flow of the working fluid: passive and active [4]. In passive SWH systems, fluid circulation occurs naturally through buoyancy forces, whereas in active systems, circulation is facilitated by pumps. The fundamental principle behind SWH operation is converting solar electromagnetic energy into thermal energy. The utilization of solar energy offers several advantages, including its abundance, environmental friendliness with minimal pollution potential [5], low investment and maintenance costs [6], and the ability to reduce reliance on fossil fuels [7]. However, solar energy's intermittent availability poses challenges for SWH applications [8]. Solar radiation is predominantly accessible during the daytime, while hot water demand often peaks during nighttime hours when solar radiation is absent. The disparity between energy availability and demand underscores the need to integrate thermal energy storage (TES) systems, enabling the storage of excess energy for future utilization. TES holds critical importance in SWH setups as it ensures a continuous supply of thermal energy to meet demand. Consequently, there is a need for ongoing development and optimization of TES designs to enhance their efficiency.

The conventional SWH typically employs water as the primary thermal energy storage medium, where energy is stored in sensible heat, resulting in temperature changes during the heating or energy release. However, conventional SWH systems suffer from several drawbacks, including significant heat loss at night, the risk of overheating in summer months [9], and the requirement of large TES volumes due to the low energy density of water [10]. In response to these challenges and to optimize solar energy utilization, phase change materials (PCM) are integrated into SWH systems, capitalizing on their capacity to store and release thermal energy via latent heat. PCMs offer several advantages, such as high energy density, a broad phase change temperature range, consistent energy intake and release at near-constant temperatures, and relatively low cost [11].

Previous studies have explored the integration of PCM in SWH systems, demonstrating improved thermal performance compared to systems lacking PCM [12]. Incorporating PCM increases the thermal energy storage capacity of SWH systems [13], particularly in forced circulation systems with vertical tanks [14]. Using PCM enhances the heat extraction from solar energy [15], while SWH tanks containing PCM capsules enhance the energy density of the overall system [16]. Furthermore, PCM integration maintains elevated temperatures during nighttime operation [17] and can lead to reduced electricity consumption in SWH systems [18]. High mass flow rates in SWH systems reduce Richardson numbers, diminishing thermal stratification [19]. Moreover, increasing the mass of PCM within the tank correlates with higher cumulative heat storage [20].

Based on prior research findings, it has been established that the integration of PCM can enhance the thermal efficiency of SWH systems. However, existing studies predominantly focus on systems utilizing vertical tanks. The thermal performance of SWH systems incorporating PCM within horizontally positioned tanks, employing a collision-type capsule arrangement, remains unexplored. In this configuration, capsules are arranged to facilitate collisions with the incoming hot water flow by aligning the water inlet axis with one of the capsule axes. Furthermore, active-type SWH systems are intricately linked to the mass flow rate of circulating water, serving as a conduit for transferring thermal energy from the collector. This study delves into the impact of heat transfer fluid (HTF) mass flow rate on the thermal dynamics of an SWH system tank containing PCM during the charging process.

2. Methods

2.1 Experimental Setup

The experiment employed a single active SWH unit comprising essential components such as a TES tank, collector, pump, and solar simulator. The TES tank served the purpose of storing thermal energy generated during the charging phase. The tank is constructed from mild steel, measuring 1220 mm in length and 250 mm in diameter. The tank was insulated with glass wool to minimize heat loss to the surroundings. Flat-plate collectors were utilized to absorb thermal energy from the energy source, with a piping system connecting the tank to the collector. A heat-resistant plastic pipe links the collector outlet to the tank input. A Rucika Kelen Green pipe facilitated flow from the tank output to the collector inlet. The tank was positioned horizontally atop the collector, which was inclined at a 15° angle relative to the floor.

The tank houses 21 capsules arranged in a collision-type configuration, serving as a heat exchanger between water and the PCM. These cylindrical capsules, made of copper, measure 1000 mm long and 1 inch in outer diameter. The RT55-type paraffin wax was utilized as the PCM, filling each capsule in its liquid state with a volume of 0.43 liters per capsule. A pump was positioned between the tank outlet and the collector inlet. The pump regulator was used to control rotation, facilitating the water mass flow rate setting via the flowmeter. Indoor experimentation was conducted utilizing a solar simulator as the energy source, boasting a total electrical power of 7.2 kW, and positioned at the same angle as the collector. The experimental equipment scheme is illustrated in Figure 1.

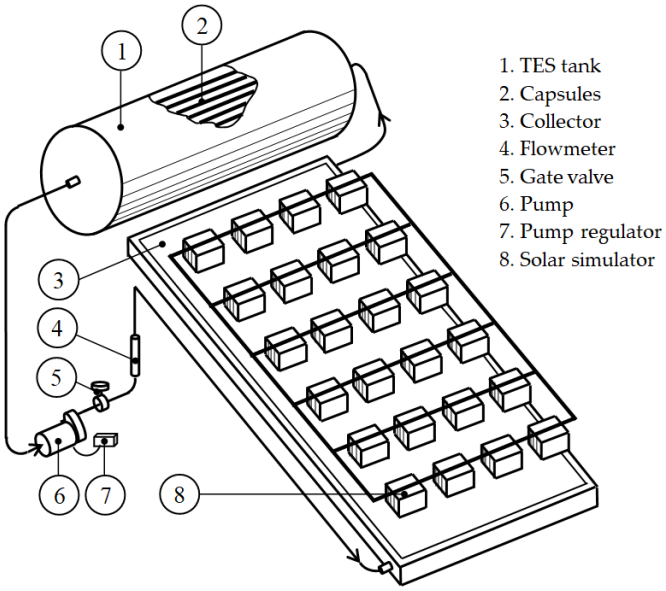

Figure 1. Experimental equipment scheme

Type K thermocouples underwent calibration procedures to ensure accuracy in temperature readings. Calibration involved assessing temperature measurements from 24 thermocouples against a standard thermometer. The results indicate a range of coefficient of determination values, with the highest at 0.9999 and the lowest at 0.9994. These findings confirm that all the thermocouples can accurately deliver the necessary temperature data. Subsequently, these thermocouples were installed on the waterside, representing the HTF and within the PCM. Twelve thermocouples were utilized for measuring water temperature, while ten were assigned for PCM measurements. These thermocouples were strategically positioned along the vertical axis of the tank, with each location spaced 406 mm apart from the tank's side. Six thermocouples were dedicated to HTF measurements within each location, and three were allocated for PCM readings. Additionally, two thermocouples were positioned at the tank's inlet and outlet to oversee the HTF's temperature at the specific locations. PCM thermocouples were also embedded within two capsules, representing the capsules' horizontal orientation, with each capsule accommodating two thermocouples. The HTF and PCM thermocouples arrangement within the tank is illustrated in Figure 2.

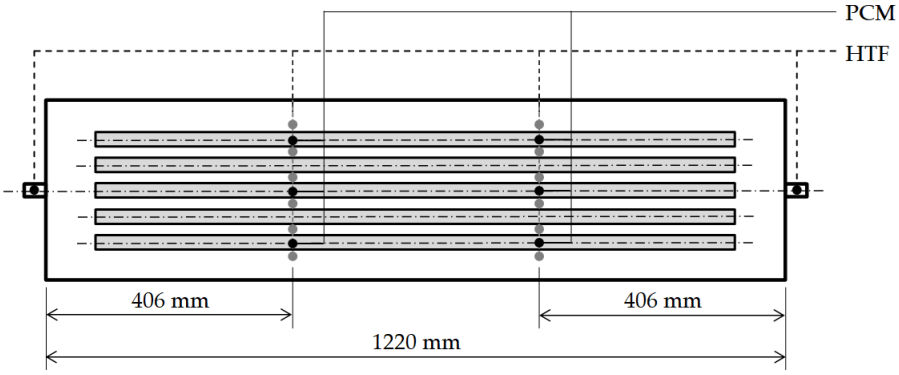

Figure 2. Location of thermocouple placement

The experiment commenced with filling the SWH system with water. The solar simulator was then activated and set to generate a heat flux of 1000 W/m^2. The solar simulator settings were adjusted through a voltage regulator, with its height adjusted relative to the collector. Subsequently, the water pump was activated and fine-tuned to achieve a mass flow rate of 0.017 kg/s. Once a steady-state flow was achieved, data acquisition procedures were initiated, and the HTF and PCM temperature recording started. Temperature data collection was conducted over 160 minutes. Upon completion of the charging stage, the

experimental protocol was repeated, following the same steps. However, the mass flow rate was adjusted to 0.013 kg/s and 0.05 kg/s for subsequent trials. Notably, temperature data collection with varying mass flow rates was conducted on the subsequent day to ensure the water temperature within the tank had returned to a cold state.

2.2 Performance Characterization

The assessment of the SWH system's effectiveness involves scrutinizing the temperature data of both the HTF and PCM throughout the charging phase. This evaluation encompasses observing the changes in HTF and PCM temperatures, as well as analyzing parameters such as instantaneous heat storage, cumulative heat storage, charging efficiency, and storage efficiency. These thermal performance metrics are examined for variations in mass flow rate.

The instantaneous heat stored refers to the heat flux occurring in the HTF within the tank at a specific moment. This parameter is determined based on factors such as the mass flow rate, the temperature difference of the HTF between the tank's inlet and outlet and the specific heat [21]. Cumulative heat stored, on the other hand, represents the summation of instantaneous heat stored throughout the charging process, and it can be computed using the following equation [22].

$$Q_{cum} = \int_0^{t_1} q_{ch,1}\, dt + \int_{t_1}^{t_2} q_{ch,2}\, dt + \cdots + \int_{t_{n-1}}^{t_n} q_{ch,n}\, dt \quad (1)$$

where Q_{cum} is the cumulative heat stored (kJ), $q_{ch,n}$ is the instantaneous heat stored at a certain time (kW), and t_n and t_{n-1} are the time instant between which instantaneous heat stored is calculated.

The charging efficiency quantifies the effectiveness of transferring thermal energy into the TES tank relative to the maximum energy that could be transferred from the start to the end of the charging process [23]. Thus, charging efficiency is determined using the following formula.

$$\eta_{ch} = \frac{T_{in} - T_o(t)}{T_{in} - T_{ini}} \quad (2)$$

where η_{ch} is the charging efficiency (%), T_{in} and $T_o(t)$ are HTF temperature at the entry and exit points of the TES tank (°C), and T_{ini} is the initial temperature of HTF in the TES tank (°C).

Storage efficiency refers to the ratio of the energy effectively stored over time compared to the maximum thermal energy that could potentially be stored in the TES tank at any given moment during the charging process. This efficiency is expressed by the following equation [23].

$$\eta_{st} = \frac{T_{avg}(t) - T_{ini}}{T_{in} - T_{ini}} \quad (3)$$

where η_{st} is the storage efficiency (%), and $T_{avg}(t)$ is the average HTF temperature in the TES tank at a specified time (°C).

3. RESULTS AND DISCUSSION

The HTF and PCM temperatures were monitored using 12 and 10 thermocouples, respectively. Temperature readings from the thermocouples were calibrated, and the averages were computed for HTF and PCM. These average temperature values were then utilized to analyze the thermal dynamics of the SWH tank during the charging process. All experiments were conducted under consistent conditions, including a heat flux of 1000 W/m^2, the presence of 21 capsules, and a charging duration of 160 minutes.

3.1 Evolution of HTF and PCM Temperature

Figure 3(a) illustrates the progression of the average HTF temperature during the heating process with a mass flow rate of 0.017 kg/s. Throughout the charging period, the HTF temperature within the tank exhibits a consistent rise. This trend can be attributed to the continuous energy supply from the solar simulator. In the beginning, the collector's absorber plate absorbs solar energy. Afterwards, this absorbed

heat is conveyed to the riser pipe, where water primarily circulates through conduction and convection processes. As a result, the water temperature within the riser pipe increases. The heated water, characterized by elevated temperatures, enters the TES tank. Convection-driven heat transfer occurs due to the temperature differential between the water originating from the collector and that present within the tank. As the charging period progresses, the water entering the tank rises, intensifying the heat transfer process and elevating the HTF temperature within the tank.

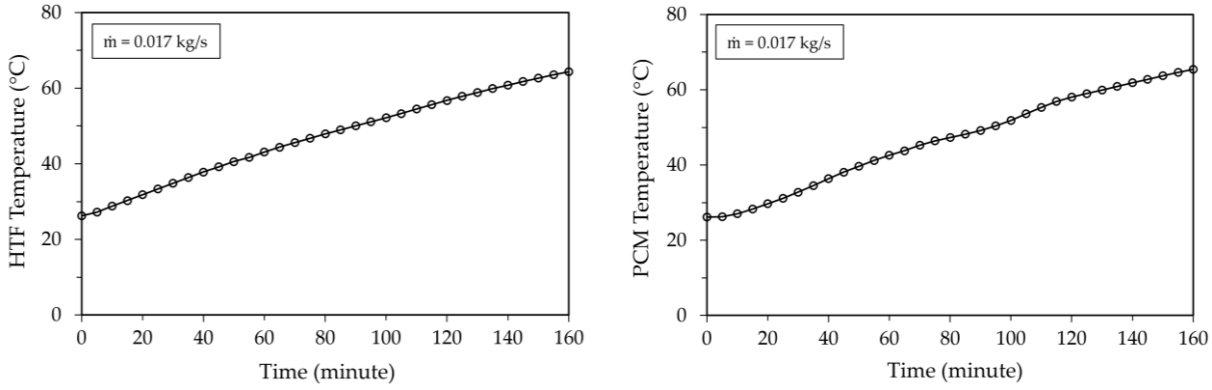

(a) (b)

Figure 3. Temperature evolution at mass flow rate of 0.017 kg/s (a) HTF (b) PCM

As depicted in Figure 3(a), the average HTF temperature at the onset of charging stood at 26.23°C, escalating to 64.38°C by the end of the process. The average heating rate of the HTF throughout charging is calculated to be 0.238 °C/minute. This metric represents the average temperature rise of the HTF observed per minute during charging. Notably, the obtained average heating rate surpasses that reported in prior research [24]. In the previous study, researchers utilized 24 capsules containing RT52 paraffin wax, structured with non-collision construction. The average heating rate achieved under similar mass flow rate conditions was 0.039 °C/minute. The ongoing experiment employs a collision capsule arrangement, ensuring that hot water from the collector collides with one of the capsules. This collision effectuates the dispersion of hot water across the tank's cross-section, thereby augmenting the average heating rate.

Figure 3(b) shows the average PCM temperature progression at a mass flow rate of 0.017 kg/s. The average PCM temperature shows a steady increase throughout the heating period. Specifically, the average temperature at the beginning and end of the charging process is recorded as 26.17°C and 65.43°C, respectively. The average heating rate during the heating phase is calculated to be 0.244 °C/min. Notably, this average heating rate exceeds that reported in previous experiments employing a non-collision capsule arrangement, which achieved a rate of 0.037 °C/minute [24].

The average temperature rise pattern observed in the PCM closely mirrors that of the HTF. As the HTF temperature within the tank increases, a temperature gradient between the HTF and the PCM ensues, housed within the capsules. Initially, heat transfer occurs primarily via convection between the flowing HTF and the capsule, followed by conduction between the capsule's outer and inner walls. The rise in wall temperature within the capsule establishes a temperature differential with the PCM, initiating heat transfer from the capsule's inner walls to the PCM, primarily through conduction. However, this heat transfer proceeds slowly due to the low thermal conductivity of the PCM, which is measured at 0.2 W/m.K [25]. Figure 3(b) shows this sluggish heat transfer process, where the PCM temperature gradually increases until approximately the 6th minute. As the amount of heat transferred from the capsule's inner walls increases, the PCM temperature rises, causing it to transition into a mushy state. Subsequently, heat transfer shifts from conduction to convection mode. As time progresses, with the accumulation of thermal energy, the PCM transitions into a liquid state. Once the PCM melts, heat transfer is primarily governed by natural convection. As the volume of melted PCM increases, buoyancy forces enhance the convective heat transfer mechanism [26]. The PCM melting process is visually depicted in Figure 4, with

a noticeable decrease in the average PCM heating rate observed from the 85th minute until the 114th minute, indicating the onset of the phase change. It is important to note that paraffin wax RT55, a non-isothermal phase change material, exhibits this phase change process [27]. Following the 114th minute, the average heating rate of the PCM experiences a resurgence.

3.2 Instantaneous Heat Stored

The main factor affecting the level of instantaneously stored heat is the difference in water temperature between the inlet and outlet of the tank, especially noticeable across different mass flow rates, as illustrated in Figure 4(a). The graphical trends observed in Figure 4(a) for the three mass flow rate variations exhibit similarities. Initially, there is a sharp rise in the temperature difference between the tank inlet and outlet, followed by a gradual decline. At the onset of the charging process, the water entering the tank is notably warmer than the HTF within the tank. Consequently, the temperature of the tank's outlet remains relatively low, resulting in a substantial temperature difference. However, as the charging period progresses, the HTF temperature within the tank gradually increases, leading to a reduction in the temperature difference.

Furthermore, Figure 4(a) illustrates that higher mass flow rates correspond to increased temperature disparities between the HTF at the entry and exit points of the tank. A greater mass flow rate induces elevated heat absorption within the collector riser pipes, consequently augmenting hot water production. As a result, this occurrence increases the temperature of the water entering the tank, thereby intensifying the temperature differential with the water exiting the tank.

The graph depicting the instantaneous heat stored during charging with varying HTF mass flow rates is shown in Figure 4(b). The graph closely reflects the pattern noticed in the temperature contrast between the inlet and outlet of the tank. This observation suggests that the primary factor influencing the calculation of instantaneous heat stored is the temperature disparity between the entry and exit sides of the tank. During the charging phase, there is a rapid increase in heat transfer, driven by the substantial temperature difference between the incoming hot water and the HTF within the tank. However, as the charging process continues, the temperature difference gradually diminishes, reducing heat transfer.

Figure 4(b) also shows that the highest instantaneous heat storage occurs at a mass flow rate of 0.05 kg/s, followed by 0.033 kg/s and 0.017 kg/s. Specifically, the peak instantaneous heat stored values for mass flow rates of 0.017 kg/s, 0.033 kg/s, and 0.05 kg/s are recorded as 1.45 kW, 1.47 kW, and 1.68 kW, respectively. Additionally, the average thermal energy per second stored for mass flow rates of 0.017 kg/s, 0.033 kg/s, and 0.05 kg/s amounts to 1 kW, 1.06 kW, and 1.14 kW, respectively. Notably, the average percentage increase in instantaneous heat stored from a mass flow rate of 0.017 kg/s to 0.03 kg/s is calculated as 6.22%, while the increase to 0.05 kg/s is 13.64%. These findings corroborate previous experiments, affirming that higher mass flow rates increase instantaneous heat storage [24]. Elevated HTF flow rates facilitate a more uniform distribution of hot water within the tank and enhance turbulence, promoting more significant heat transfer.

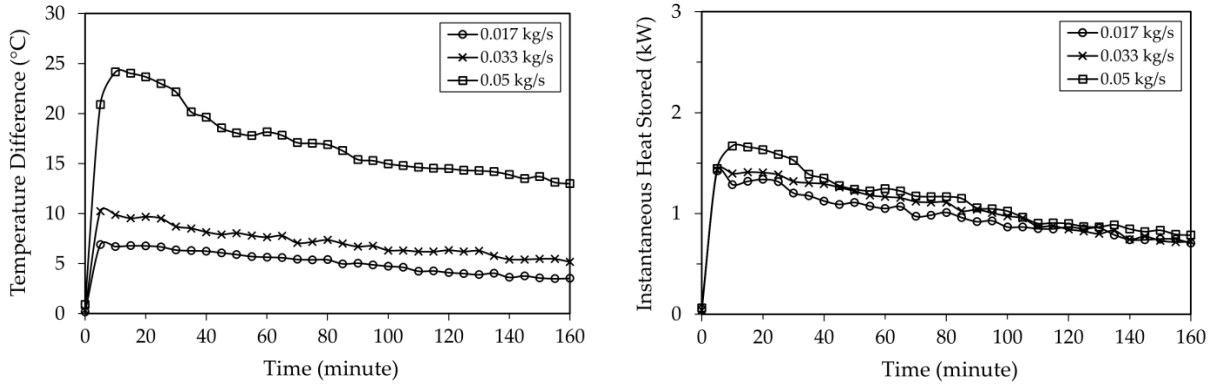

(a) (b)

Figure 4. (a) Temperature difference at inlet and outlet of the tank (b) instantaneous heat stored

3.3 Cumulative Heat Stored

Figure 5 illustrates the total amount of heat accumulated within the storage tank at different mass flow rates. This parameter is derived by summing up the instantaneous heat stored values obtained from Figure 4(b). It is evident that the cumulative heat stored increases across all variations with prolonged charging durations. Towards the conclusion of the charging process, the tank demonstrates cumulative heat stored values of 9.62 MJ, 10.2 MJ, and 11.09 MJ, respectively, for mass flow rates of 0.017 kg/s, 0.033 kg/s, and 0.05 kg/s. The percentage increase in cumulative heat stored during charging from a mass flow rate of 0.017 kg/s to 0.03 kg/s is 6.05%, while the increase to 0.05 kg/s amounts to 15.34%. The heightened mass flow rate augments heat transfer within the tank, increasing the cumulative heat stored [28]. The rapid phase change process observed for more significant mass flow rates also contributes to the elevated cumulative heat stored values [29]. A rapid phase change in the PCM signifies a substantial amount of thermal energy contained within the TES tank.

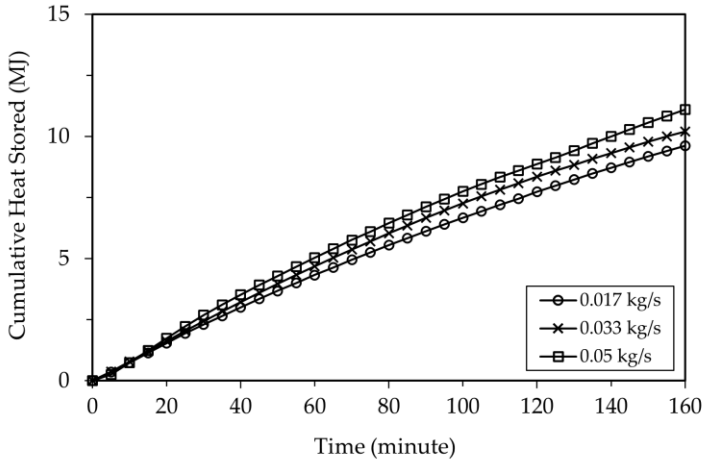

Figure 5. Cumulative heat stored with various mass flow rate

Cumulative heat storage is an essential parameter in thermal energy storage within storage tanks, offering insights into the time needed to achieve a specific cumulative heat level. For instance, as depicted in Figure 5, it can be inferred that the duration required to attain a cumulative heat stored of 6 MJ at mass flow rates of 0.017 kg/s, 0.033 kg/s, and 0.05 kg/s is 88 minutes, 79 minutes, and 74 minutes, respectively.

According to Equation (1), the cumulative heat stored over time equals the sum of the instantaneous heat stored. The temperature differential between the incoming and outgoing water in the tank determines the instantaneous heat stored. Consequently, the highest possible total heat storage occurs when the inlet and outlet water temperatures are equal.

3.4 Charging Efficiency

Figure 6 illustrates the evolution of charging efficiency within the SWH tank across three different mass flow rate variations. As previously mentioned, charging efficiency in a SWH tank is determined by comparing the instantaneous heat transfer with the maximum potential heat transfer achievable during the charging process. Across all mass flow rate variations, a consistent trend is observed wherein charging efficiency starts high at the onset of charging, gradually diminishing as the charging duration progresses.

Equation (2) indicates that the numerator signifies the temperature contrast between the HTF entering and leaving the tank. At the same time, the denominator signifies the disparity between the HTF entering the tank and its initial temperature within the tank. At the commencement of charging, the numerator value closely matches the denominator value, resulting in a charging efficiency close to 100%. This phenomenon indicates that an efficient heat transfer process is initially occurring.

However, as heating the SWH proceeds, the temperature difference between the HTF inlet and outlet decreases, leading to a decline in the system's charging efficiency. This reduction in temperature difference is attributed to heat transfer within the tank, causing the HTF temperature to rise,

subsequently elevating the outlet HTF temperature; consequently, with prolonged charging durations, both the HTF temperature within the tank and the HTF temperature leaving the tank increase, resulting in a decrease in charging efficiency.

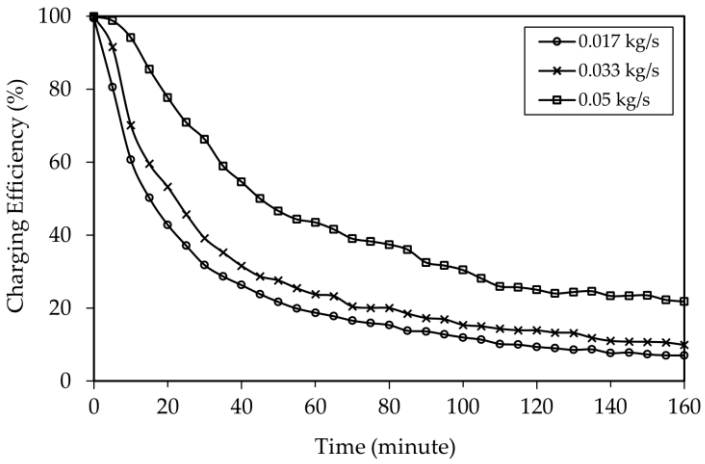

Figure 6. Charging efficiency for various mass flow rate

Figure 6 confirms a direct correlation between mass flow rate and charging efficiency, indicating that higher mass flow rates lead to greater charging efficiency. After the charging process, the charging efficiency values for mass flow rates of 0.017 kg/s, 0.03 kg/s, and 0.05 kg/s are recorded as 7.06%, 9.89%, and 21.77%, respectively. Additionally, the average charging efficiency throughout the heating phase for mass flow rates of 0.017 kg/s, 0.03 kg/s, and 0.05 kg/s are calculated as 22.05%, 27.87%, and 44.41%, respectively. Transitioning from a mass flow rate of 0.017 kg/s to 0.03 kg/s results in a 23.84% increase in charging efficiency, while an increase to 0.05 kg/s leads to a significant 97.36% enhancement.

A higher mass flow rate indicates an incredible flow velocity, elevating the Reynolds number. The Nusselt number, a dimensionless parameter linked to convection heat transfer, increases with a higher Reynolds number. Consequently, a higher mass flow rate results in a more significant Nusselt number, facilitating increased heat transfer. These findings align with previous computational fluid dynamics (CFD) analysis research. Moreover, as the HTF temperature within the tank rises over time, the potential temperature difference between the HTF at the tank's inlet and the average tank temperature diminishes [30]. The CFD analysis mirrors the findings of this study, depicted in Figure 6. However, the discrepancy in the charging efficiency trend between the CFD analysis and the research data lies in the smoother curve of the former. This smoothness arises from assuming a constant temperature for the water entering the tank in the CFD analysis. Conversely, in our experiment, the temperature of the inlet water varies, resulting in fluctuations in the charging efficiency graph.

The cumulative heat stored depicted in Figure 5 exhibits a distinct characteristic compared to the charging efficiency graph illustrated in Figure 6. With prolonged charging durations, the cumulative heat stored steadily rises, whereas the charging efficiency declines. This trend arises from the definition of cumulative heat stored as the aggregate of instantaneously stored heat during charging, leading to an increase over time. Conversely, the charging efficiency diminishes with extended charging periods due to the diminishing temperature differential between the tank's inlet and outlet, as indicated by Equation (2). This trend stems from the rising water temperature within the tank.

3.5 Storage Efficiency

The storage efficiency delineates the extent to which thermal energy can be stored in the TES tank relative to the maximum energy change during the charging process. Unlike charging efficiency, storage efficiency is directly correlated with the temperature differential between the instantaneous average HTF temperature within the tank and the initial temperature. The progression of storage efficiency across the three mass flow rate variations is depicted in Figure 7. The graph illustrates a consistent trend wherein

storage efficiency increases over time. Irrespective of the mass flow rates, prolonged charging durations increase the tank's thermal energy accumulation. This stored thermal energy corresponds to the cumulative heat stored at any moment [23]. As depicted in Figure 5, the cumulative heat stored progressively increases with time, consequently amplifying storage efficiency.

Figure 7 demonstrates that as mass flow rates increase, storage efficiency also rises. After the charging process, storage efficiency values for mass flow rates of 0.017 kg/s, 0.03 kg/s, and 0.05 kg/s are reported as 64.72%, 74.44%, and 78.28%, respectively, with corresponding average values of 43.1%, 53.81%, and 59.03%. The average increase in storage efficiency from a mass flow rate of 0.017 kg/s to 0.03 kg/s is calculated at 24.86%, while the increase for a mass flow rate of 0.05 kg/s amounts to 36.95%.

As the mass flow rate increases, more significant flow fluctuations occur within the tank, improving heat transfer. This enhancement leads to an elevation in HTF temperature within the tank, resulting in more excellent stored heat.

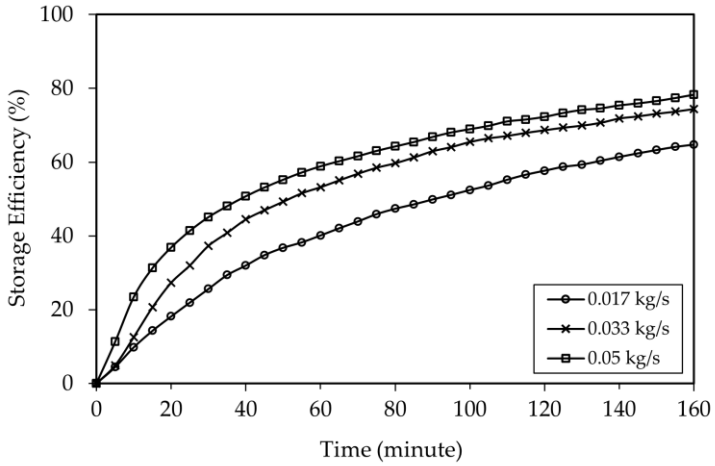

Figure 7. Storage efficiency for various mass flow rate

4. CONCLUSION

This study explores the thermal dynamics of an SWH system incorporating water and PCM as thermal energy storage mediums, with varied mass flow rates observed over a 160-minute charging period. Increasing the mass flow rate from 0.017 kg/s to 0.05 kg/s results in a 13.64% rise in instantaneous heat stored, a 15.34% increase in cumulative heat stored, and a 36.95% enhancement in storage efficiency. These findings underscore the significant influence of mass flow rate on the thermal characteristics of the SWH system, indicating that higher mass flow rates contribute to improved thermal performance. Future research endeavors should further explore this relationship by increasing the range of mass flow rate variations.

REFERENCES

[1] A. Raihan, "An overview of the energy segment of Indonesia: present situation, prospects, and forthcoming advancements in renewable energy technology," *J. Technol. Innov. Energy*, vol. 2, no. 3, pp. 37–63, 2023, doi: 10.56556/jtie.v2i3.599.

[2] B. P. Resosudarmo, J. F. Rezki, and Y. Effendi, "Prospects of Energy Transition in Indonesia," *Bull. Indones. Econ. Stud.*, vol. 59, no. 2, pp. 149–177, 2023, doi: 10.1080/00074918.2023.2238336.

[3] E. Erdiwansyah *et al.*, "Investigation of availability, demand, targets, and development of renewable energy in 2017–2050: a case study in Indonesia," *Int. J. Coal Sci. Technol.*, vol. 8, no. 4, pp. 483–499, 2021, doi: 10.1007/s40789-020-00391-4.

[4] A. Jamar, Z. A. A. Majid, W. H. Azmi, M. Norhafana, and A. A. Razak, "A review of water heating system for solar energy applications," *Int. Commun. Heat Mass Transf.*, vol. 76, pp. 178–187, 2016, doi: 10.1016/j.icheatmasstransfer.2016.05.028.

[5] M. Shirinbakhsh, N. Mirkhani, and B. Sajadi, "Optimization of the PCM-integrated solar domestic

hot water system under different thermal stratification conditions," *Energy Equip. Syst.*, vol. 4, no. 2, pp. 271–279, 2016.

[6] S. ed D. Fertahi, A. Jamil, and A. Benbassou, "Review on Solar Thermal Stratified Storage Tanks (STSST): Insight on stratification studies and efficiency indicators," *Sol. Energy*, vol. 176, pp. 126–145, 2018, doi: 10.1016/j.solener.2018.10.028.

[7] F. G. Uctug and A. Azapagic, "Life cycle environmental impacts of domestic solar water heaters in Turkey: The effect of different climatic regions," *Sci. Total Environ.*, vol. 622–623, pp. 1202–1216, 2018, doi: 10.1016/j.scitotenv.2017.12.057.

[8] G. Murali, K. Mayilsamy, and T. V. Arjunan, "An experimental study of PCM-incorporated thermosyphon solar water heating system," *Int. J. Green Energy*, vol. 12, no. 9, pp. 978–986, 2015, doi: 10.1080/15435075.2014.888663.

[9] S. Bouadila, M. Fteïti, M. M. Oueslati, A. Guizani, and A. Farhat, "Enhancement of latent heat storage in a rectangular cavity: Solar water heater case study," *Energy Convers. Manag.*, vol. 78, pp. 904–912, 2014, doi: 10.1016/j.enconman.2013.07.094.

[10] M. H. Abokersh, M. Osman, O. El-Baz, M. El-Morsi, and O. Sharaf, "Review of the phase change material (PCM) usage for solar domestic water heating systems (SDWHS)," *Int. J. Energy Res.*, vol. 42, no. 2, pp. 329–357, 2018, doi: 10.1002/er.3765.

[11] R. Gulfam, P. Zhang, and Z. Meng, "Advanced thermal systems driven by paraffin-based phase change materials – A review," *Appl. Energy*, vol. 238, pp. 582–611, 2019, doi: 10.1016/j.apenergy.2019.01.114.

[12] I. Al-Hinti, A. Al-Ghandoor, A. Maaly, I. Abu Naqeera, Z. Al-Khateeb, and O. Al-Sheikh, "Experimental investigation on the use of water-phase change material storage in conventional solar water heating systems," *Energy Convers. Manag.*, vol. 51, no. 8, pp. 1735–1740, 2010, doi: 10.1016/j.enconman.2009.08.038.

[13] O. Ibrahim, F. Fardoun, R. Younes, and H. Louahlia-Gualous, "Review of water-heating systems: General selection approach based on energy and environmental aspects," *Build. Environ.*, vol. 72, pp. 259–286, 2014, doi: 10.1016/j.buildenv.2013.09.006.

[14] Z. Wang, F. Qiu, W. Yang, and X. Zhao, "Applications of solar water heating system with phase change material," *Renew. Sustain. Energy Rev.*, vol. 52, pp. 645–652, 2015, doi: 10.1016/j.rser.2015.07.184.

[15] P. Feliński and R. Sekret, "Experimental study of evacuated tube collector/storage system containing paraffin as a PCM," *Energy*, vol. 114, pp. 1063–1072, 2016, doi: 10.1016/j.energy.2016.08.057.

[16] M. Y. Abdelsalam, P. Sarafraz, J. S. Cotton, and M. F. Lightstone, "Heat transfer characteristics of a hybrid thermal energy storage tank with Phase Change Materials (PCMs) during indirect charging using isothermal coil heat exchanger," *Sol. Energy*, vol. 157, pp. 462–476, 2017, doi: 10.1016/j.solener.2017.08.043.

[17] W. Wu *et al.*, "Experimental study on the performance of a novel solar water heating system with and without PCM," *Sol. Energy*, vol. 171, pp. 604–612, 2018, doi: 10.1016/j.solener.2018.07.005.

[18] S. Lu, T. Zhang, and Y. Chen, "Study on the performance of heat storage and heat release of water storage tank with PCMs," *Energy Build.*, vol. 158, pp. 1770–1780, 2018, doi: 10.1016/j.enbuild.2017.10.059.

[19] H. Huang *et al.*, "An experimental investigation on thermal stratification characteristics with PCMs in solar water tank," *Sol. Energy*, vol. 177, pp. 8–21, 2019, doi: 10.1016/j.solener.2018.11.004.

[20] M. Nadjib, N. Caroko, T. Thoharudin, and I. Pranoto, "Application of Phase-Change Material in an Active-Type Solar Water Heater: Effect of Void Fraction," in *AIP Conference Proceedings*, AIP Publishing, 2023. doi: 10.1063/5.0181908.

[21] N. Nallusamy, S. Sampath, and R. Velraj, "Experimental investigation on a combined sensible and latent heat storage system integrated with constant/varying (solar) heat sources," *Renew. Energy*, vol. 32, no. 7, pp. 1206–1227, 2007, doi: 10.1016/j.renene.2006.04.015.

[22] A. Agarwal and R. M. Sarviya, "An experimental investigation of shell and tube latent heat

storage for solar dryer using paraffin wax as heat storage material," *Eng. Sci. Technol. an Int. J.*, vol. 19, no. 1, pp. 619–631, 2016, doi: 10.1016/j.jestch.2015.09.014.

[23] R. Majumdar and S. K. Saha, "Effect of varying extent of PCM capsule filling on thermal stratification performance of a storage tank," *Energy*, vol. 178, pp. 1–20, 2019, doi: 10.1016/j.energy.2019.04.101.

[24] M. Nadjib, T. H. A. Santosa, A. D. Sentosa, and D. Mukhlisin, "Pengaruh Variasi Debit Air Terhadap Unjuk Kerja Termal Tangki Pemanas Air Tenaga Surya yang Berisi Phase-Change Material," *JMPM (Jurnal Mater. dan Proses Manufaktur)*, vol. 6, no. 1, pp. 1–10, 2022, doi: 10.18196/jmpm.v6i1.14795.

[25] Rubitherm Technologies GmbH, "Technisches Datenblatt RT55," Berlin, 2020. [Online]. Available: www.rubitherm.com

[26] A. Sarı and K. Kaygusuz, "Thermal and heat transfer characteristics in a latent heat storage system using lauric acid," *Energy Convers. Manag.*, vol. 43, no. 18, pp. 2493–2507, 2002, doi: 10.1016/S0196-8904(01)00187-X.

[27] A. Trp, "An experimental and numerical investigation of heat transfer during technical grade paraffin melting and solidification in a shell-and-tube latent thermal energy storage unit," *Sol. Energy*, vol. 79, no. 6, pp. 648–660, 2005, doi: 10.1016/j.solener.2005.03.006.

[28] G. Li, "Energy and exergy performance assessments for latent heat thermal energy storage systems," *Renew. Sustain. Energy Rev.*, vol. 51, pp. 926–954, 2015, doi: 10.1016/j.rser.2015.06.052.

[29] W. Lin, Z. Ling, X. Fang, and Z. Zhang, "Experimental and numerical research on thermal performance of a novel thermal energy storage unit with phase change material," *Appl. Therm. Eng.*, vol. 186, no. December 2020, p. 116493, 2021, doi: 10.1016/j.applthermaleng.2020.116493.

[30] A. S. Ramana, R. Venkatesh, V. Antony Aroul Raj, and R. Velraj, "Experimental investigation of the LHS system and comparison of the stratification performance with the SHS system using CFD simulation," *Sol. Energy*, vol. 103, pp. 378–389, 2014, doi: 10.1016/j.solener.2014.02.009.